

CFD simulations of transient load change on a high head Francis turbine

Ken-Robert G. Jakobsen¹, Martin Aasved Holst²

¹ Senior Technical Consultant, EDRMedeso AS

² Manager – Technical Services, EDRMedeso AS

EDRMedeso AS, Leif Tronstads plass 4, 1337 Sandvika, NORWAY

ken-robert.g.jakobsen@edrmedeso.com, martin.aasved.holst@edrmedeso.com

Abstract. Motivated by the importance of better understanding the structural integrity of high-head hydraulic turbines operating at intermittent conditions, complete 360° steady-state and transient simulations of a Francis turbine are presented in this paper. The main target of the work has been to investigate different numerical approaches such as mesh deformation for different operating conditions. Steady-state simulations were performed at the best efficiency point (BEP) and used as initial conditions for the transient simulations considering load rejection from BEP to part load (BEP2PL) and during load acceptance from BEP to high load (BEP2HL). Simulation results were compared with experimental data available for the Francis-99 project where close agreement was found for the mesh independent solution. The transient load analyses showed general trends in accordance with the measurement reports, especially for the pressure in vaneless space that is of high importance regarding RSI effects. Some deviations were identified for the net head at load rejection for which further investigations will be conducted. All CFD simulations were performed at model scale with ANSYS CFX v. 17 at either 96 or 120 cores (2.60 GHz). The immersed boundary technique was tested during the initial stages of the project, but had to be abandoned due to severe memory requirements. Pressure amplitudes and other instantaneous results were not considered.

Abbreviations

- BEP - Best Efficiency Point
- BEP2HL - Load acceptance
- BEP2PL - Load rejection
- CFD - Computational Fluid Dynamics
- GV - Guide Vane
- HL - High Load
- NTNU - Norwegian University of Science and Technology
- PL - Part Load
- RANS - Reynolds Averaged Navier-Stokes Equations
- RSI - Rotor-Stator Interaction
- RPM - Revolutions Per Minute
- SST - Shear Stress Transport



1. Introduction

The work presented here has been conducted as part of the HiFrancis project and specifically aiming for the second Francis-99 workshop where the focus lays on steady and transient numerical simulations of the Francis-99 hydraulic turbine located at the Water Power Laboratory at NTNU. Measurements of several experimental studies have been made available for comparison with the numerical results obtained by the workshop participants [1]. The Francis-99 project consists of a total of three strongly coupled workshops, the final one scheduled to take place in 2018. An in-depth description of the problem at hand together with an overview of the existing experimental and numerical findings from the Francis-99 workshops conducted so far can be found in [2].

The future hydropower systems will require operations with increased flexibility due to the introduction of intermittent energy sources such as wind and solar. This includes large and fast ramping rates and more frequent load changes that must be part of the future design criteria for new high head Francis turbines as the systems will be subjected to higher stress levels and consequently more fatigue. More efficient and more accurate numerical simulations will help providing better insight into how these new load histories affect the structural integration of the turbines. A necessary aid in this work is the ever-increasing computer power providing both faster results and the ability to run more expensive simulations. The latter has also been one of the main motives for the present study considering transient CFD simulations of the complete 360° Francis-99 turbine. These types of analyses are rare due to their high level of computational intensity and will in that sense hopefully bring new and fruitful information to the work aiming at better understanding the Francis turbine.

A thorough overview of the status of numerical modeling and simulation of hydraulic turbines at transient operating conditions today is given in [3].

2. Model setup

All simulations presented in this document were performed on a three-dimensional computational domain with a 360° turbine where the fluid behavior was obtained by solving the transient Reynolds averaged Navier-Stokes equations. The software used was ANSYS CFX v. 17.

Figure 1 shows the computational domain obtained by extracting the confined fluid domain from the Francis-99 turbine geometry. The main boundary conditions driving the fluid flow have been indicated:

- Inlet: Mass flow.
- Outlet: Pressure outlet.
- Walls: No-slip.
- Interface type: Frozen and transient rotor.

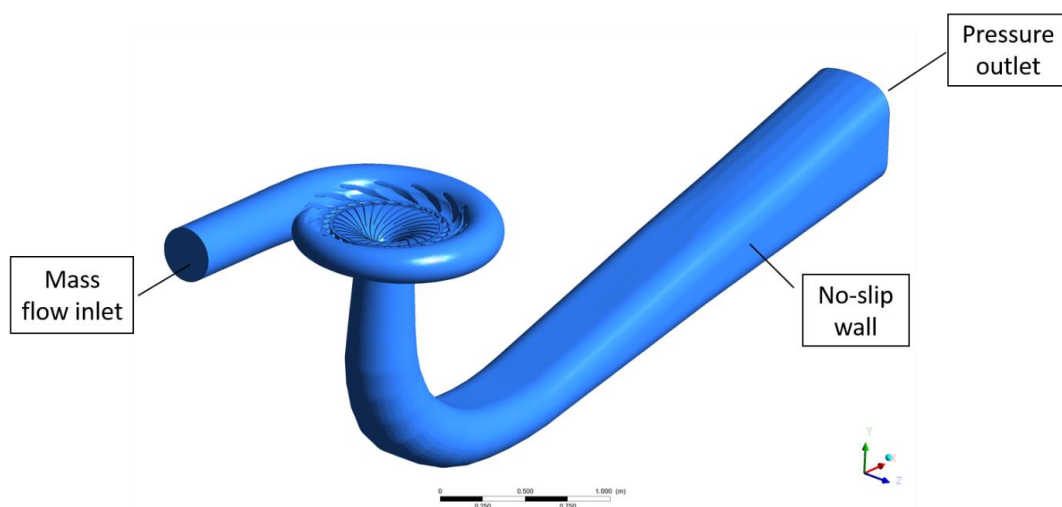


Figure 1. Computational domain.

In addition, the leakage gaps leading to the labyrinth seals were included by applying mass flow outlets at those locations. The latter was estimated to be 0.2% of the mass flow at BEP [4]. In [5], further details on the effect of including the leakage gaps can be found.

The working fluid in the analyses was incompressible water with density equal $999.8 \text{ [kg/m}^3\text{]}$ and kinematic viscosity of $9.57\text{e-}7 \text{ [m}^2\text{/s]}$.

2.1. Computational mesh

All simulations were performed on spiral casing meshes consisting of tetrahedral elements in the bulk flow and hexahedral elements in the near-wall regions capturing the boundary layer effects. On a general note, more tetrahedral elements are required compared with hexahedral elements to achieve mesh independency. The upside, however, is that they are very flexible and will easily mesh complex structures such as the present configuration. The latter is also a great advantage for the transient load scenarios where the rotation of the guide vanes were obtained utilizing mesh deformation following the specifics given in Table 1. It should also be noted that the immersed boundary method was tested for which the geometries subjected to motion are represented by momentum sources rather than resolved by computationally expensive meshes. However, this approach was abandoned due to very high memory requirements experienced with the present software.

As this work also aims at providing simulation procedures that are easily reproducible and at a reasonable cost post simulation, it was decided to focus solely on spiral casing meshes made of tetrahedrons, visualized in Figure 2. In the runner and draft tube, hexahedral elements were utilized for all cases. Details on mesh resolution are given in chapter 3.

Table 1. Mesh motion model.

Model	Option
Mesh motion	Displacement diffusion
Mesh stiffness	Increase near small volumes (model exponent = 1)
Guide vane displacement	Specified displacement (cylindrical components)

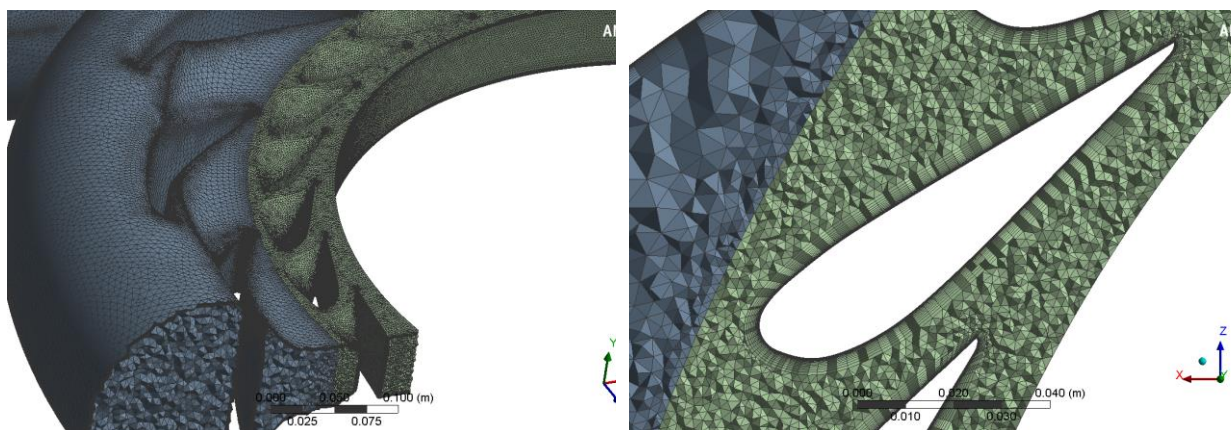


Figure 2. Computational domain with mesh consisting of tetrahedral elements (Case 3/8, see chapter 3). Left: Mesh at part of volute. Right: Boundary layer at one guide vane shown at a horizontal section.

2.2. Turbulence model

The industry standard SST turbulence model was applied to all simulations providing an accurate near-wall flow solution through the traditional k- ω model as well as in the free stream using the k- ϵ model with additional transportation term for shear stress. For this mixing to take place, the SST model does indeed require a fine mesh resolution near the no-slip boundaries and chapter 4. shows that this was accounted for in the present simulations by adjusting the first node from the wall (y^+).

3. Simulation cases

The simulation cases performed in the present study have been listed in Table 2, covering both the mesh independence study and comparison with experiments (Case 1 – 9) as well as transient load cases (Case 9 and 10). All simulations include the full three-dimensional solution of the Navier-Stokes equations with a 360° turbine in steady-state (frozen rotor) or transient (rotating rotor) configurations. In accordance with the procedures for the available experimental data [1], the transient simulations see a turbine operating at a constant rotational speed of 333rpm throughout the investigation, while the inlet mass flow for the transient load cases between stationary operation points follow the same history as defined below for the guide vane movement. The simulation time steps have been defined as function of number of guide vanes (28) and angular speed of turbine (ω):

$$dt = \frac{2\pi}{28\omega N} \quad (1)$$

where N was chosen to ensure a fixed number of turbine rotations. The transient load cases include guide vane rotation to model either *load acceptance* or *load reduction* defined as:

1. Load acceptance: Increase turbine output from BEP to HL by opening the guide vanes from 9.84 degrees (BEP2HL). Mass flow linearly increased from 0.2 m³/s (BEP) to 0.24 m³/s (HL).
2. Load reduction: Decrease turbine output power from BEP to PL by closing the guide vanes from 9.84 degrees (BEP2PL). Mass flow linearly decreased from 0.2 m³/s (BEP) to 0.14 m³/s (PL).

Table 2. Simulation cases.

Case #	Type	Number of nodes (x10 ⁶)	Time step [s]
1	Steady-state	7	-
2	Steady-state	22	-
3	Steady-state	42	-
4	Steady-state	100	-
5	Transient	7	1x10 ⁻⁴
6	Transient	22	1x10 ⁻⁴
7	Transient	42	1x10 ⁻⁴
8	Transient	100	1x10 ⁻⁴
9	Transient, BEP2HL	42	8x10 ⁻⁴
10	Transient, BEP2PL	42	8x10 ⁻⁴

The angular velocity of the guide vanes was derived from the operation scheme used in the experiments (see Figure 3) supplemented by their notes in [1] stating that: “At time $t=1$ s, the guide vanes were set to open/close to perform transient conditions. After certain time, the guide vanes reached to set value of angle (i.e., 6.72° or 12.43°) then steady state condition was followed”.

Resulting from this, the load acceptance and rejection had to be run for operational times of 1.8s and 2.5s, respectively. In comparison, the BEP transient simulation was run for 0.54s, or three runner rotations, after which steady pressure signals were achieved after approximately half a rotation. The BEP transient result file was used as starting point for the load acceptance/rejection cases.

Briefly anticipating the course of the events, the final transient load cases defined in Table 2 were performed on the computational mesh consisting of 42 million cells as this gave mesh independent results. Further details are given in the subsequent chapters.

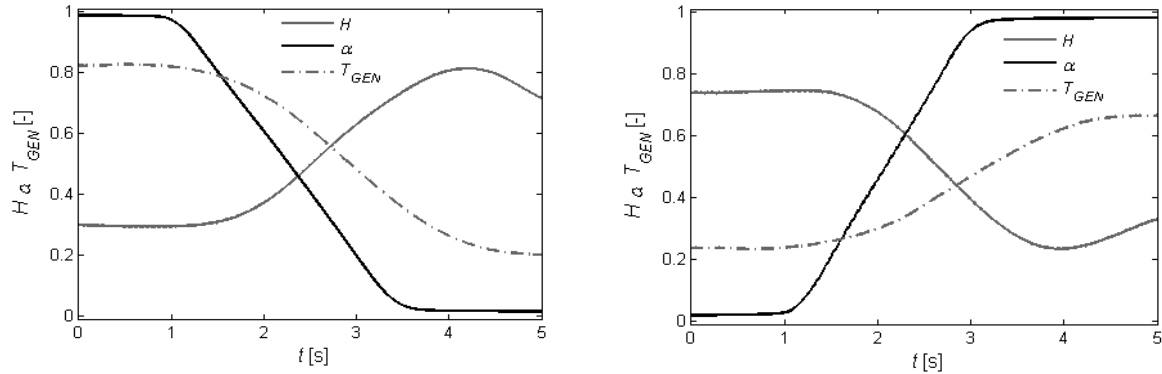


Figure 3. Operating schemes of guide vanes (α) in experiments [1]. Left: Load reduction (BEP2PL). Right: Load acceptance (BEP2HL).

4. Analysis results

The present chapter includes the analysis results obtained from the simulation cases defined in Table 2. These are presented in the following fashion:

1. Mesh sensitivity study
2. Comparison with experiments
3. Transient load change.

In accordance to the available experimental data, the main results of interest have been the net head and generator torque. The net head includes the casing inlet pressure and draft tube pressure and is defined as [1]:

$$Net\ head = \frac{P_{1abs} - P_{2abs}}{\rho g} + \frac{v_1^2 - v_2^2}{2g} + z \quad (2)$$

4.1. Mesh sensitivity study

Ranging from approximately 7 to 100 million computational nodes, four different mesh sizes were tested for the BEP stationary operating condition. In general, the mesh study was performed by refining both the bulk flow and boundary layer (lower y^+) for each case, except between Case 3 and 4 where only the bulk flow resolution was increased. This is summarized in Table 3. It is here the average y^+ values in the respective computational domains that have been reported. Obviously, as y^+ is velocity dependent, this value will vary greatly in such a complex flow path as seen in the present configuration. Using the global average value is thus considered a representative measure for the turbulence model of choice.

Table 3. Mesh resolutions.

Case #	Number of nodes (*10 ⁶)	Average y+ Volute [-]	Average y+ Runner [-]	Average y+ Draft tube [-]
1	7.4	41.1	158.6	71.2
2	22.4	24.5	35.5	21.9
3	42.5	2.8	2.8	1.6
4	100.1	3.1	3.0	1.4

As seen in Table 4 and the corresponding convergence plot in Figure 4, the results for net head and torque indicate that mesh independency for the 360° turbine was obtained at 42 million nodes for the frozen rotor (Case 3). The same conclusion was reached in the transient rotor simulations in Case 5 to 8. Also included is a comparison between torque based on the torque definition and on change in angular momentum from the inlet to the outlet of the runner. The latter derives from the Euler turbine equations and is proportional with $U \cdot C_u$, where U is the velocity of the runner and C_u is the tangential velocity at the inlet/outlet of the runner. These parameters should converge on the same value and is used to measure whether the mesh captures the velocity field accurately or not.

Based on the above, it was decided to utilize the Case 3/7 mesh for the transient load simulations. Note, however, that the boundary layer was not refined for the final mesh resolution.

Table 4. Mesh sensitivity study (BEP)

Case #	Net head [Nm]	Torque to generator [Nm]
1	12.44	643.6
2	12.32	635.0
3	11.88	617.5
4	11.86	616.5
5*	12.58	652.0
6*	12.45	643.1
7*	11.99	624.2
8*	11.97	622.9

**Mass flow average*

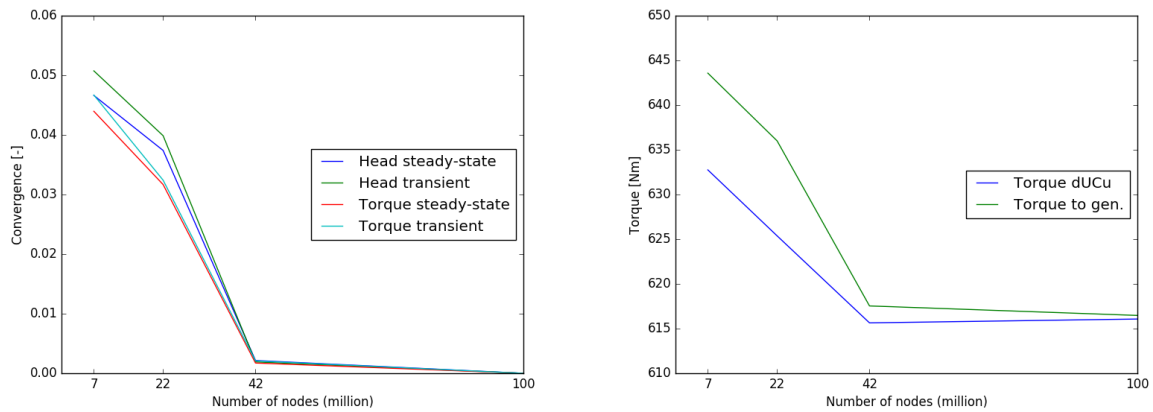


Figure 4. Left: Convergence plot of mesh sensitivity study for steady-state and transient simulation cases. Convergence is defined as $\left| \frac{\varphi_n}{\varphi_{100mill}} - 1 \right|$, where φ is the variable in question. Right: Torque to gen. vs Torque ΔUC_u .

4.2. Comparison with experiments

Considering steady-state and transient simulations at the 42 million nodes mesh configuration (Case 3/7), Table 5 and Table 6 show the results obtained for both frozen and transient rotor together with the corresponding experimental values as extracted from [1]. The locations of the vaneless space probes (VL and VL2) are shown in Figure 5. In Figure 6, velocity and pressure contours for Case 7 have been presented.

In general, the analysis results show good agreement with the experimental data at all validation points for the steady-state simulations as well as when applying a transient rotor. Directly comparing the two methods, some variables improved slightly while other showed increased differences with the experiments when going from stationary to transient rotor. However, with deviations in the order of 0-1% except for the VL1 pressure in vaneless space at 3.8%, the overall accuracy was considered high and providing the necessary confidence in the analysis methodology of choice to continue with load acceptance and rejection as presented in the subsequent chapter.

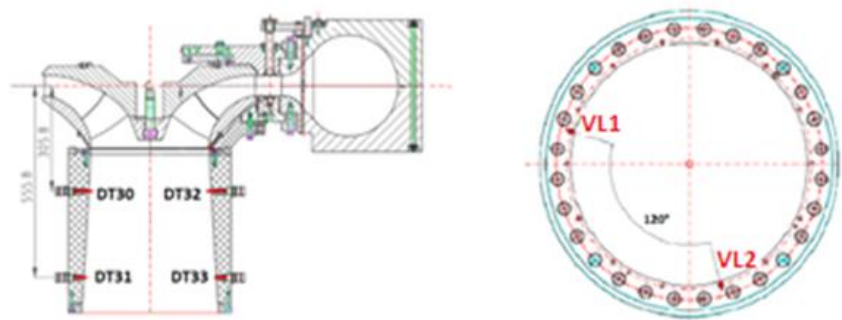


Figure 5. Location of pressure sensors. Only vaneless space (VL1 and VL2) considered here [6].

Table 5. Global measurement variables at BEP (steady-state and transient simulations).

Case #	Net head [m]		Torque to generator [Nm]		Inlet pressure [kPa]		Outlet pressure [kPa]		Hydraulic efficiency [%]	
Exp.	11.94	Dev. [%]	616.1	Dev. [%]	215.57	Dev. [%]	111.13	Dev. [%]	92.39	Dev. [%]
3	11.88	-0.5	617.5	0.2	217.95	1.1	111.83	0.6	92.41	0.0
7*	11.99	0.4	624.2	1.3	219.09	1.6	111.83	0.6	92.51	0.1

*Mass flow average values

Table 6. Pressure in vaneless space at BEP (transient simulation).

Case #	VL1 [kPa]	VL2 [kPa]
Exp.	168.0	164.2
7*	174.3	164.2
Deviation [%]	3.8	0.0

*Mass flow average values

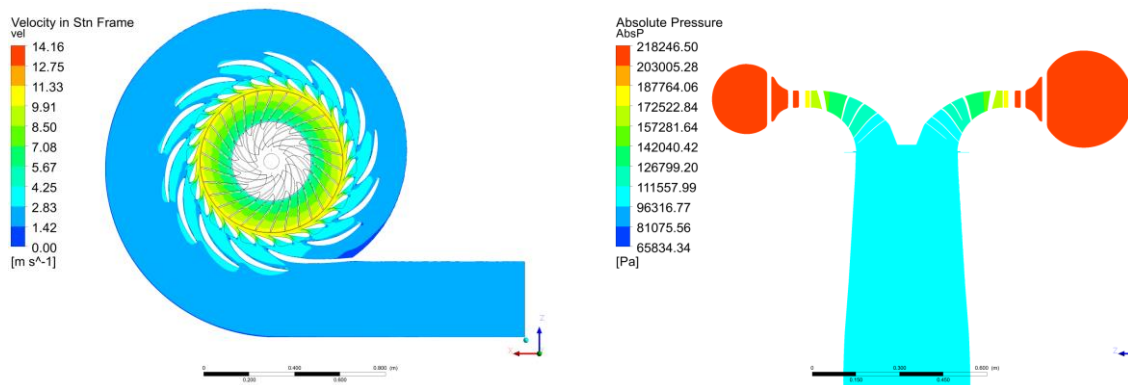


Figure 6. Case 7 results. Left: Velocity contours in stationary frame on horizontal mid plane. Right: Absolute pressure on vertical mid plane.

4.3. Transient load change

This chapter considers the load acceptance and load rejection analyses denoted as Case 9 (BEP2HL) and Case 10 (BEP2PL), respectively. As for the stationary load simulations, these results have also been subject to comparison with the experimental measurements in [1]. The transient rotor results obtained in Case 7 were used as initial values and the simulations were terminated at the time where the guide vanes found their final position. Note also that the mass flow specified at the inlet saw a linear change with time during the simulations, following the operating scheme seen in Figure 3. A close-up of the mesh around one of the guide vanes is given in Figure 7 showing its final two positions after rotating approximately 3 degrees in either direction, i.e. post load acceptance and load rejection.

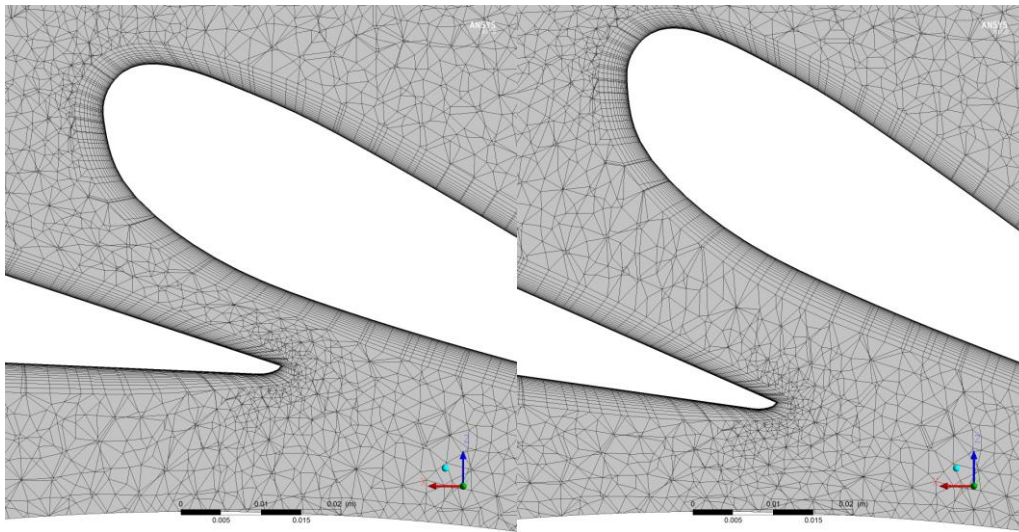


Figure 7. Final GV position during load rejection (left) and load acceptance (right).

Figure 8 and Figure 9 show the net head and the pressure in vaneless space (VL2) for load acceptance and load rejection, respectively. As amplitudes and instantaneous results have not been subject in the present section, second order polynomials were used to compare with the existing measurements as they provided the overall trends in the highly transient data pool. In agreement with the comparison data, the net head decreased during opening of the guide vanes (BEP2HL) and increased during load rejection (BEP2PL), while the VL2 pressures saw the opposite behavior. Clearly, the trends are matching with the experiments, especially for the VL2 pressure that is of high importance regarding RSI. However, the time history of the net head during load rejection did not agree with the behavior of the experimental data at a satisfactory level. The percentage deviations given for both cases in Figure 10 show that all results are still within 6% of the comparison data.

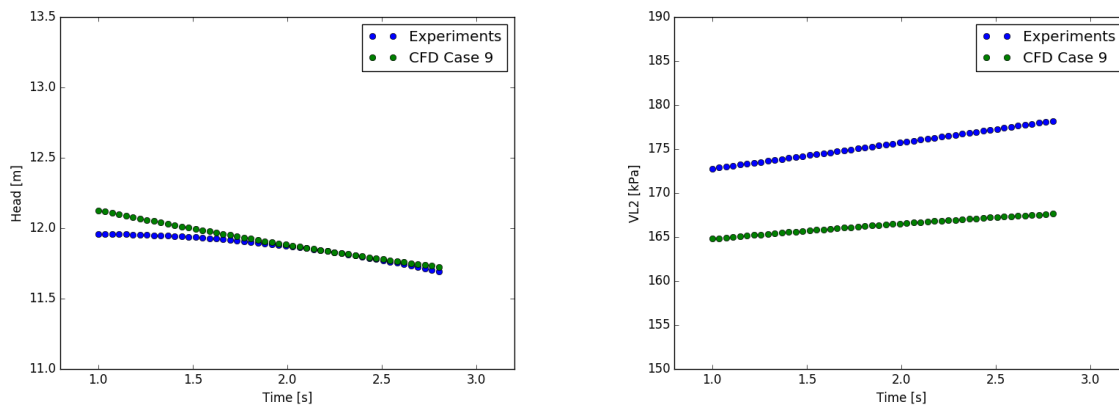


Figure 8. Net head (left) and VL2 pressure (right) during transient load operation at BEP2HL (Case 9).

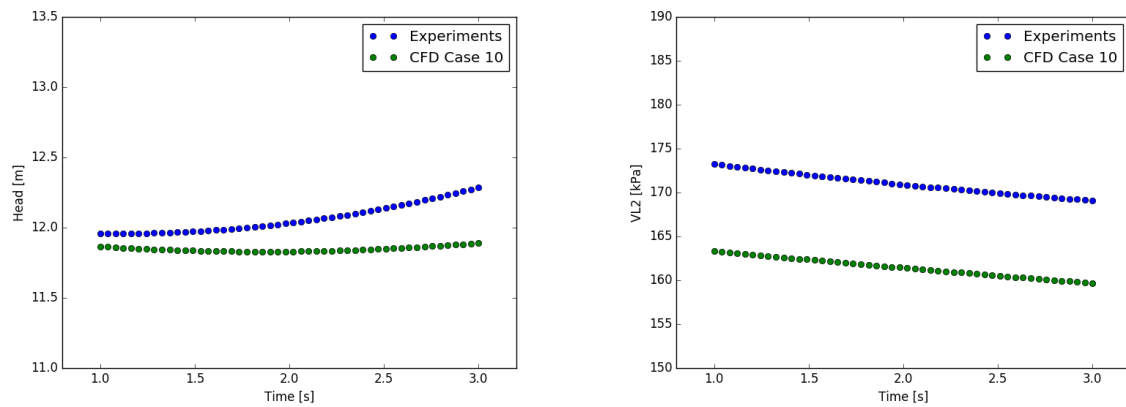


Figure 9. Net head (left) and VL2 pressure (right) during transient load operation at BEP2PL (Case 10).

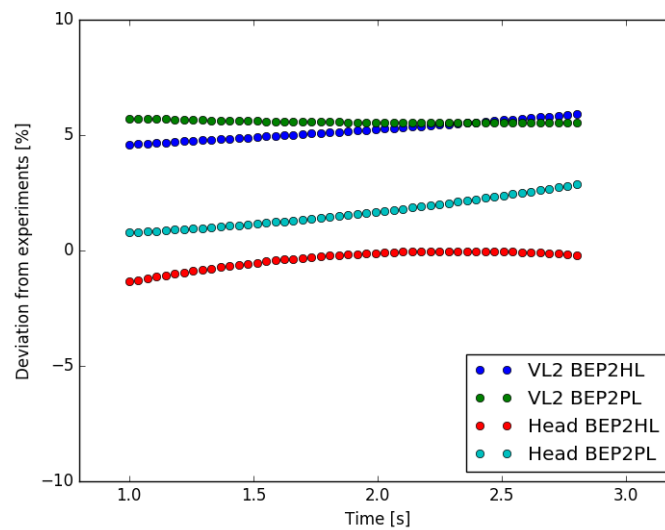


Figure 10. Percentage deviation from experiments (Case 9 & 10).

Illustrated by streamlines initiated at the runner/draft tube interface, Figure 11 shows the vortex rope in draft tube after end of guide vane rotation for both load rejection and load acceptance. While there were no flow circulations of significance in the draft tube at BEP (not shown), strong swirls of opposite direction were generated during opening and closing of the guide vanes. These are known effects in the literature when considering stationary load conditions [2]. The BEP2HL case shows a more defined swirl with higher fluid velocities in accordance with the higher mass flow loading.

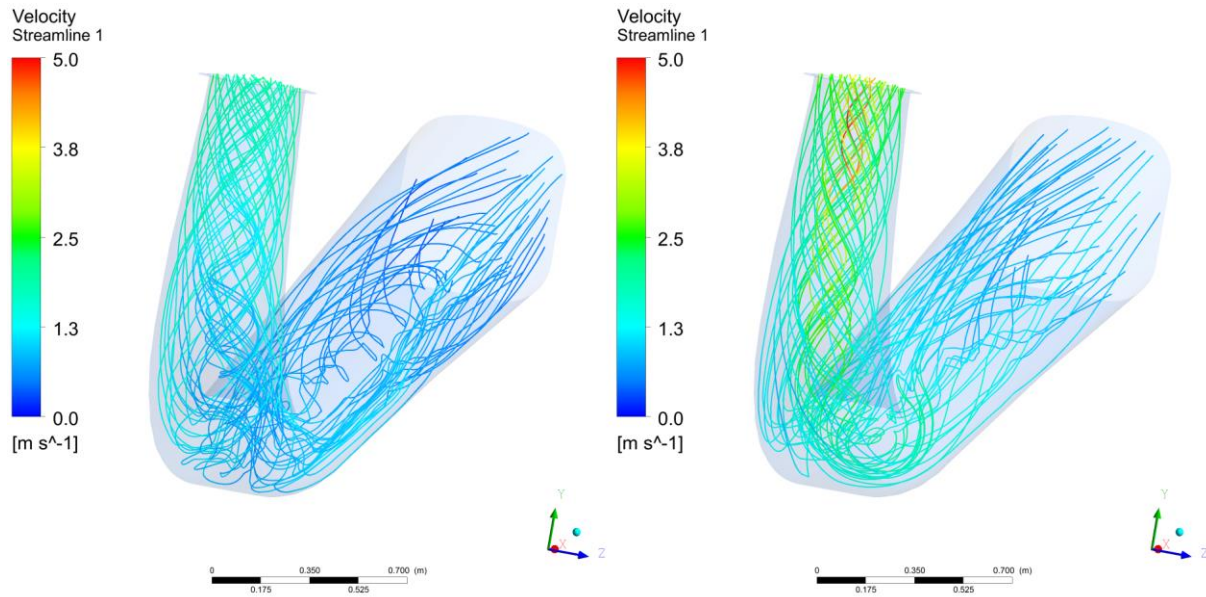


Figure 11. Streamlines from runner/draft tube interface at end of guide vane rotation. Left: BEP2PL, right: BEP2HL.

Representing flow field in blade passage, Figure 12 and Figure 13 give the velocity in rotating frame and the velocity in stationary frame, respectively. The contours have been visualized on an isosurface going through the center of the runner and following its out-of-plane direction. The absolute pressure in the runner is seen in Figure 14, clearly experiencing the familiar RSI pressure behavior at the circumference of the domain [2].

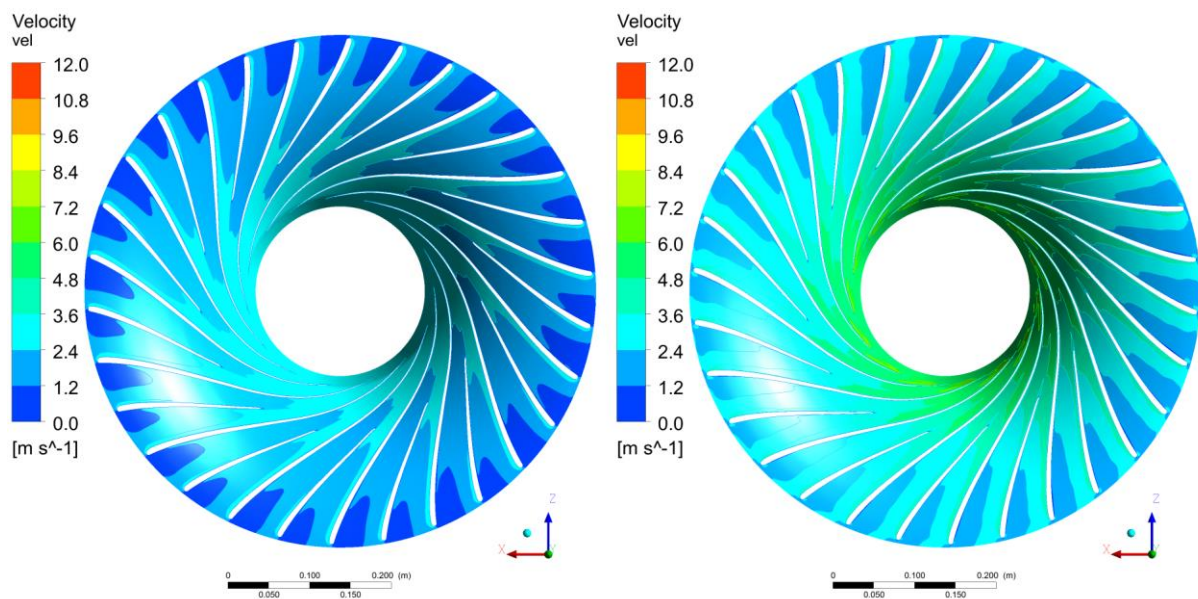


Figure 12. Velocity in rotating frame at end of guide vane rotation. Left: BEP2PL, right: BEP2HL.

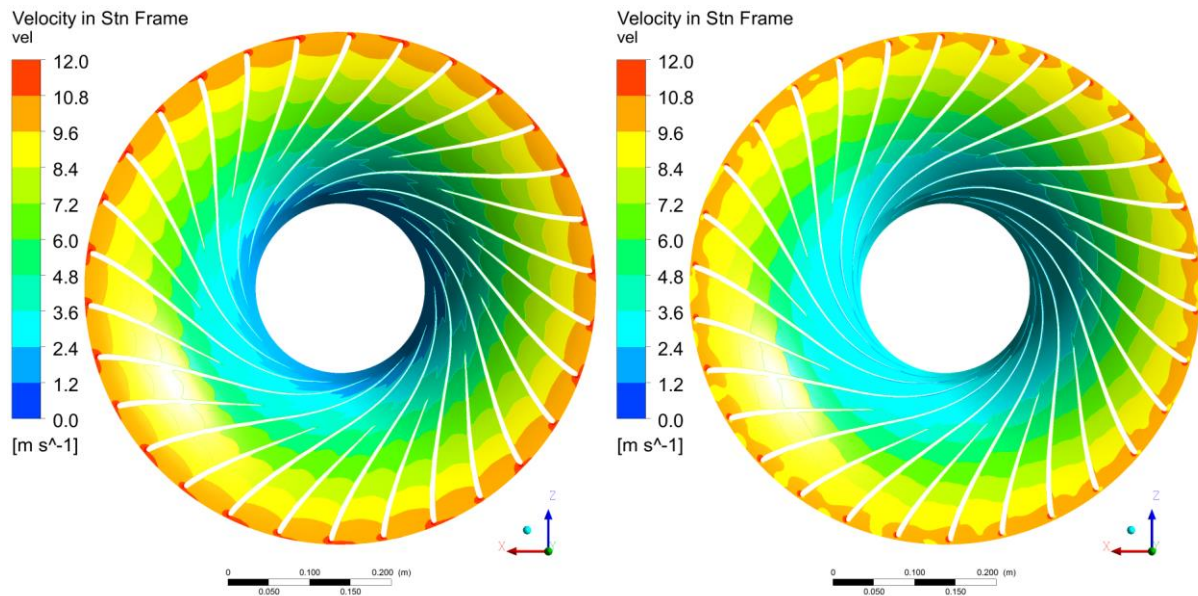


Figure 13. Velocity in stationary frame at end of guide vane rotation. Left: BEP2PL, right: BEP2HL.

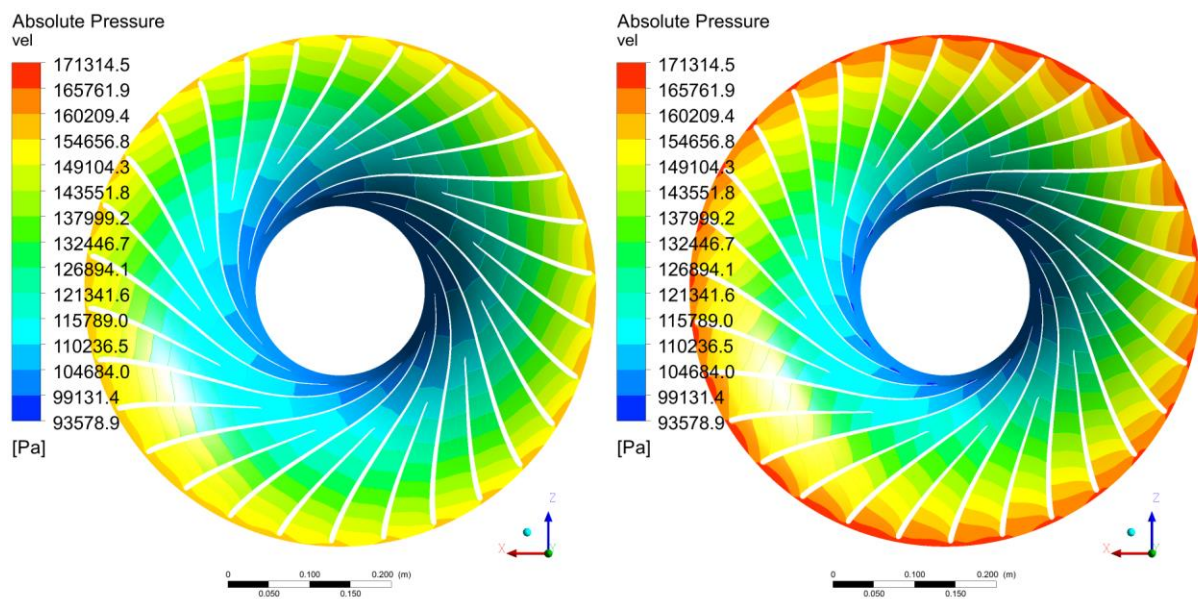


Figure 14. Absolute pressure at end of guide vane rotation. Left: BEP2PL, right: BEP2HL.

5. Concluding remarks

Steady-state and transient CFD simulations have been performed on the full 360° Francis-99 hydraulic turbine, including load acceptance and rejection utilizing mesh deformation. The work was performed for the second Francis-99 workshop and as part of the HiFrancis project and the results have been compared to the existing measurements performed at the Water Power Lab at NTNU.

The main findings from the mesh dependency study and comparison with experimental data were as follows:

- A mesh independent solution was reached for a mesh with approximately 42 million nodes and near wall y^+ values in the order of 3 in the spiral casing and runner. Tetrahedral elements were used in the spiral casing.
- The comparison between torque and torque based on ΔU_{Cu} proved that the velocity field was captured at sufficient accuracy as the difference between the two was low ($<1\%$) for the mesh independent solution.
- Average values for global variables such as net head, torque, inlet pressure, outlet pressure and hydraulic efficiency were in general predicted very well. The results improved further by including a transient rotor. Pressure amplitudes have not been subject to investigation in the present paper.

During load acceptance and rejection, the guide vane rotation was performed in accordance with the operating scheme reported in [1]. The transient results obtained at the mesh independent solution was used as initial condition with the main findings as follows:

- In general, good agreement was found when comparing the trends of the global measurement variables with results being within 6% off from the experiments. More specifically and important for capturing the effects of RSI, the pressure in vaneless space (VL2) agreed very well with the experiments.
- The initial deviations on absolute values were in accordance with the results seen for the stationary load cases used as starting conditions. However, net head during load rejection did not follow the experimental values at a satisfactory level.

The observation made for the net head at load rejection will be investigated further, including alterations such as applying a pressure condition at the volute inlet rather than explicitly specifying the mass flow. The latter will be in closer resemblance with both the experiments as well as real life situations. Other known deviations from the experiments are that the simulations were performed with one single upstream pressure probe, while the experimental data reports an average of four circumferentially placed probes at that location. Also, updated guide vane position from the experiments shows a deviation of about 0.02 degrees.

At the time of writing, further investigations are currently ongoing as part of the HiFrancis project.

References

- [1] NTNU, "Francis-99 Second Workshop," [Online]. Available: <https://www.ntnu.edu/nvks/test-case>.
- [2] C. Trivedi, M. J. Cervantes, B. K. Gandhi and O. G. Dahlhaug, "Experimental and Numerical Studies for a High Head Francis Turbine at Several Operating Points," *Journal of Fluids Engineering*, vol. 135, 2013.
- [3] C. Trivedi, M. J. Cervantes and O. G. Dahlhaug, "Numerical Techniques Applied to Hydraulic Turbines: A Perspective Review," *Applied Mechanics Reviews*, vol. 68, 2016.
- [4] C. Trivedi, *NTNU, Email and phone correspondance throughout project*.
- [5] J. Schiffer, H. Benigni and H. Jaberg, "Analysis of the leakage behaviour of Francis turbines and its impact on the hydraulic efficiency - A validation of an analytical model based on CFD-results," *Jornal of Fluids Engineering*, 2016.
- [6] K. Kloster, "Pressure pulsation inside a Francis turbine runner (Master Thesis)," NTNU, 2016.